Research Article

Nanofibrous *p-n* Junction and Its Rectifying Characteristics

Jian Fang, Xungai Wang, and Tong Lin

Australian Future Fibres Research and Innovation Centre, Deakin University, Geelong, VIC 3220, Australia

Correspondence should be addressed to Tong Lin; tong.lin@deakin.edu.au

Randomly oriented tin oxide (SnO_2) nanofibers and poly(3,4-ethylenedioxythiophene)-poly(styrenesulfonate)/polyvinylpyrrolidone (PEDOT:PSS/PVP) nanofibers were prepared by a two-step electrospinning technique to form a layered fibrous mat. The current-voltage measurement revealed that the fibrous mat had an obvious diode-rectifying characteristic. The thickness of the nanofiber layers was found to have a considerable influence on the device resistance and rectifying performance. Such an interesting rectifying property was attributed to the formation of a *p-n* junction between the fibrous SnO_2 and PEDOT:PSS/PVP layers. This is the first report that a rectifying junction can be formed between two layers of electrospun nanofiber mats, and the resulting nanofibrous diode rectifier may find applications in sensors, energy harvest, and electronic textiles.

1. Introduction

Porous media have diverse applications ranging from filtration and gas/liquid adsorption to optics, electronics, sensors, and biomedicine. They can be prepared by different techniques with pores controllable on *macro-*, *meso-,* or *micro-*scales [1]. Nanofibrous materials represent a special class of porous media, made of nanofibers or nanowires, often in a form of thin fibrous structures. The large specific surface area, high porosity, and excellent pore interconnectivity have significantly enhanced their application performance. In electronic and energy areas, nanofibrous materials have been used as electrodes, separators, or active layers for development of batteries [2], solar cells [3], sensors [4], and power generators [5].

Despite the semiconducting characteristic of some nanofibers, nanofibrous materials are predominantly prepared to have homogeneous properties throughout the structure. Heterogeneous electrical property, such as diode *p-n* junction and rectifying effect, would enable a fibrous material to control the carrier transport, which creates opportunities to develop novel multifunctional nanofibrous materials and devices. Recently, a fully porous *p-n* junction prepared from porous silicon has been reported [6]. *p-n* junction carbon nanotube networks have also been prepared using a partial doping method [7]. However, *p-n* junction and rectifying effect formed between two layers of different nanofibers have been little reported in the research literature.

In our recent study, we found that, when tin oxide (SnO_2) nanofibers and poly(3,4-ethylenedioxythiophene)-poly(styrenesulfonate)/polyvinylpyrrolidone (PEDOT:PSS/PVP) nanofibers were prepared separately by an electrostatic spinning, that is, electrospinning [8–12], technique to form a layered fibrous mat, a device made of this mat showed an interesting rectifying behavior and *p-n* junction characteristic. This fibrous device may find applications for textile electronics or rectifier for fibrous energy harvesters. In this paper, we report on the preparation of this novel nanofibrous device and its rectifying performance.

2. Experimental Details

2.1. Materials. Tin(II) chloride dehydrate ($SnCl_2 \cdot 2H_2O$), PVP, N,N-dimethylformamide (DMF), acetonitrile, and ethanol were purchased from Sigma and used as received. Tetrabutylammonium hexafluorophosphate (Bu_4NPF_6) was obtained from Fluka, and 1.3 wt% aqueous PEDOT:PSS solution (Baytron P) was kindly provided by H.C. Starck.

$SnCl_2$-PVP solution was prepared by dissolving PVP (M_w = 1,300,000) and $SnCl_2 \cdot 2H_2O$ into a mixture of ethanol and DMF (1/2, v/v). The concentration of PVP and

$SnCl_2$ in the solution was 30.0 wt% and 21.0 wt%, respectively. PEDOT:PSS-PVP solution was prepared by adding 1 g PVP (M_w = 360,000) and 2.5 mL DMF into 4 mL Baytron P.

2.2. Electrospinning. Electrospinning was performed using a purpose made setup consisting of a high voltage power supply, a syringe pump, and a grounded collector [13]. During electrospinning, the spinning solution was loaded into a 5 mL plastic syringe with a 21-gauge metal needle. A syringe pump (KD Scientific) was used to control the flow rate, and a high voltage was applied between the needle and a grounded metal collector, using a high voltage power supply (ES3P-5W, Gamma High Voltage).

$SnCl_2$/PVP nanofibers were electrospun under an applied voltage = 15 kV, spinning distance = 18 cm, flow rate = 0.6 mL/h. PEDOT:PSS/PVP nanofibers were directly electrospun (applied voltage = 18 kV, spinning distance = 15 cm, flow rate = 0.2 mL/h) from the second solution onto the surface of the SnO_2 nanofiber mat to form a second nanofibrous layer.

2.3. Device Fabrication. To prepare a rectifier device, $SnCl_2$/PVP nanofibers were electrospun and deposited onto a thin aluminium plate (steps are illustrated in Figure 2(a)). SnO_2 nanofibers were then obtained by calcinating the as-electrospun nanofibers together with the aluminium substrate at 250°C for one hour and 500°C for 5 hours to remove all the organic components. Subsequently, PEDOT:PSS/PVP nanofibers were formed on the top of the SnO_2 nanofiber layer, followed by sputter-coating a layer of gold (Au) on the PEDOT:PSS/PVP nanofiber mat.

2.4. Characterizations. Morphology of the nanofibers was examined on a field emission scanning electron microscope (SEM, Supra V55). All samples were gold coated (Bal-tec SCD50 sputter coater), and the images were taken at an acceleration voltage of 5 kV. The fiber diameter was calculated using image processing software (Image Pro-Plus 4.5). X-ray diffraction (XRD) results were obtained on a diffractometer (PANalytical XRD) using Cu radiation 1.54 Å. The samples were analysed at room temperature with sampling intervals of 0.02° and a scanning rate of 0.25°/min. The average size of SnO_2 crystals was calculated according the Scherrer equation ($D = 0.9\lambda/\beta \cos\theta$), where λ is the wavelength of X-ray, θ is the diffraction angle, and β is the full width half max of the (211) diffraction peak. An electrochemical workstation (CHI760D) was used to measure the *I-V* characteristics and electrical impedance spectra (EIS) of the devices. The LUMO and HOMO energy levels of PEDOT:PSS/PVP nanofiber mat were also measured on CHI760D by a cyclic voltammetry (CV) method [14]. Acetonitrile was used as solvent and Bu_4NPF_6 (0.1 mol/L) as the support electrolyte. All the measurements were performed at room temperature.

3. Results and Discussion

Figure 1(a) shows the SEM image of the $SnCl_2$/PVP nanofibers. The fibers had uniform morphology with an average

diameter of 674 nm. After the calcination treatment, the average diameter reduced to 368 nm (Figure 1(b)). Although the fiber surface became very rough (Inset image in Figure 1(b)) after the treatment, the fibers still retained the fibrous form without breakage.

The X-ray diffraction (XRD) patterns of the $SnCl_2$/PVP and SnO_2 nanofibers are shown in Figure 1(c). The as-electrospun $SnCl_2$/PVP nanofibers showed no obvious crystal peak, indicating an amorphous state. In contrast, strong diffraction peaks corresponding to SnO_2 crystal planes of (110), (101), (200), (211), (220), (002), (310), (112), (301), (202), and (321) were found in the spectrum, which matched well with the standard XRD data of SnO_2 (JCPDS-41-1445) [15]. This confirms that $SnCl_2$ has been converted to SnO_2, and PVP has been removed from the fibers after the calcination treatment. Based on the (211) phase, the average SnO_2 crystal size was calculated by the Scherrer equation to be about 14 nm.

Figure 1(d) shows the SEM image of PEDOT:PSS/PVP nanofibers. The fibers looked uniform with a diameter of 103 ± 22 nm. Normally, the average diameter of electrospun nanofibers is about 200 nm. The smaller average diameter for the PEDOT:PSS/PVP nanofibers was attributed to the increased charge density and associated enhancement in fiber stretching when ionic PEDOT:PSS was present in the electrospinning solution [16].

The process for fabrication of the nanofibrous device is illustrated in Figure 2(a). After electrospinning (Figure 2(a)(I)), $SnCl_2$/PVP nanofibers on an aluminum substrate were subjected to a calcination treatment to get pure SnO_2 nanofibers (Figure 2(a)(II)). Another layer of PEDOT:PSS/PVP nanofibers was then deposited directly onto the SnO_2 layer (Figure 2(a)(III)). After sputter-coating a thin layer of gold on the top surface of the PEDOT:PSS/PVP nanofiber mat (Figure 2(a)(IV)), a simple electronic device was finally formed. When the Au electrode was connected to the working electrode of the workstation, while the Al electrode was linked to the counter and the reference electrodes, and voltage was swept from −5.0 to +5.0 V, the device *I-V* curve was recorded. As shown in Figure 2(b), the *I-V* curves of the nanofibrous device showed a typical rectifying feature. The forward current increased with increasing the bias voltage, while the reverse current was maintained at a very low value regardless of the change of voltage. When the connection was reversed, the rectifying effect changed the polarity. These results clearly indicate that the nanofibrous device has a typical diode rectifying characteristic [17].

The thickness of nanofibers layer was found to play a key role in the rectifying behaviour. In this study, the nanofiber layer thickness was controlled through electrospinning time. For the SnO_2 nanofiber layer, short circuit occurred when the layer thickness was less than 3 μm. However, the intrinsic stiffness of SnO_2 made it difficult to handle during the device fabrication, and when the SnO_2 nanofiber layer was thicker than 6 μm, the SnO_2 layer was hard to connect with the electrode. Based on this, the nanofibrous devices were made by keeping the SnO_2 nanofiber layer thickness at 4 μm to achieve stable rectifying behaviour.

(a)

(b)

(c)
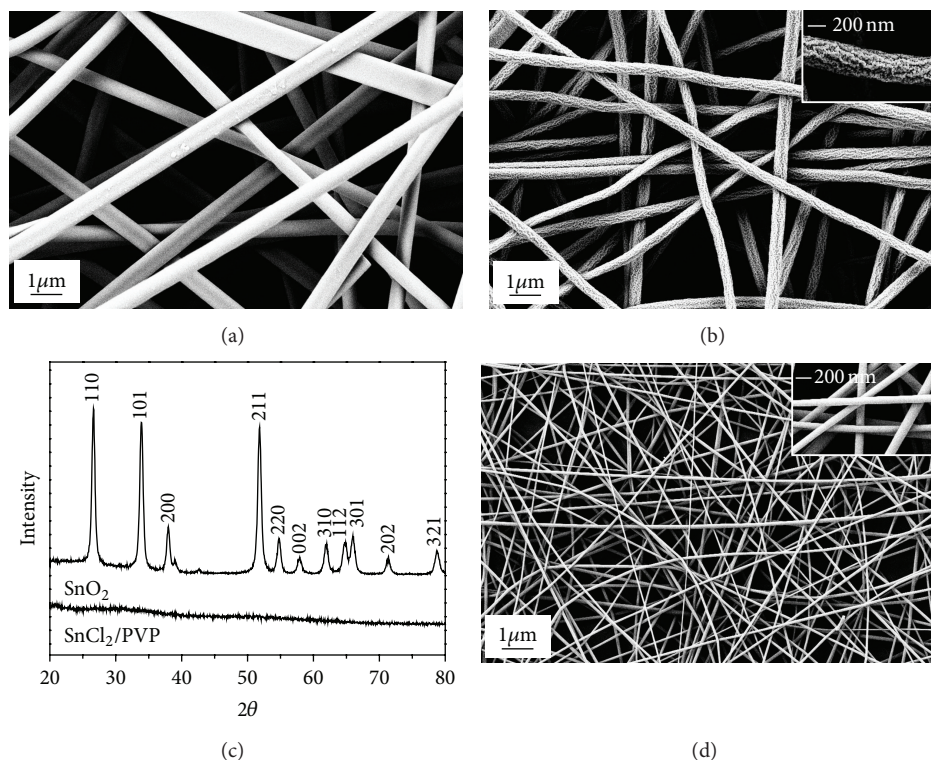

(d)

Figure 1: SEM images of (a) as-spun SnCl$_2$/PVP nanofibers and (b) SnO$_2$ nanofibers after calcination (the inset is a high magnification image), (c) XRD pattern of the SnCl$_2$/PVP and SnO$_2$ nanofibers, and (d) SEM image of the PEDOT:PSS/PVP nanofibers (the inset is a high magnification image).

In comparison to the SnO$_2$ nanofiber layer, the PEDOT:PSS/PVP layer was more flexible to adjust its thickness. Figure 2(b) also shows the effect of PEDOT:PSS/PVP fibrous layer thickness on the I-V characteristic. With increasing the thickness from 4.8 μm to 11.6 μm, the forward current decreased, while the reverse current was almost unchanged.

Based on the I-V curves, the rectification ratio (R) and turn-on voltage of these devices were measured. R was calculated by $R = I^+/I^-$ (where I^+ is the forward current at forward bias of 5 V and I^- is the leaking current at reverse bias of -5 V). For the device with the PEDOT:PSS/PVP nanofiber layer thickness of 4.8, 7.9, and 11.6 μm, the R value was 48, 35, and 35, respectively, and the minimum forward voltage required to turn on the junction was 2.78, 2.94, and 3.07 V, respectively. Normally, the turn-on voltages for commercial silicon and germanium diodes are 0.7 and 0.3 V, respectively. The higher turn-on voltage of the nanofibrous devices was presumably due to the complex fibrous structure.

To verify the role of the nanofiber layers in the rectifying effect, the I-V characteristic of single nanofiber layer, either from SnO$_2$ or PEDOT:PSS/PVP, was also measured. As shown in Figure 2(c), a linear feature was obtained for the PEDOT:PSS/PVP nanofiber mat when it was sandwiched between Au electrodes, indicating the Ohmic contact between the PEDOT:PSS/PVP nanofiber mat and the gold. For SnO$_2$ nanofiber mat, a nonlinear I-V curve was formed when two Al electrodes were used, but without rectifying behavior. This is probably because of the weak bonding

between the SnO$_2$ nanofiber and the electrodes. When a thin layer of metal aluminium was inserted between the SnO$_2$ and PEDOT:PSS/PVP nanofiber layers, the rectifying effect disappeared also. Therefore, the SnO$_2$ and PEDOT:PSS/PVP nanofiber layers and their close contact are essential for the formation of the rectifying effect.

SnO$_2$ has been reported to have n-type semiconductor characteristic with a wide bandgap ($\sim$ 3.5 eV) [18, 19]. The conduction and valance bands of SnO$_2$ are -4.5 and -8.0 eV, respectively [20]. Since the size of SnO$_2$ nanofibers is far beyond the range showing the size effect, the effect of nanofibrous structure on the band energy level can be ignored.

It has been established that PEDOT:PSS is a p-type electroactive polymer with tuneable electrical conductivity [21]. The pure PEDOT:PSS was reported to have the lowest unoccupied molecular orbital (LUMO) and the highest occupied molecular orbital (HOMO) energy levels of -3.5 and -5.2 eV [22]. However, the presence of PVP in the PEDOT:PSS nanofibers could affect the energy levels of PEDOT:PSS/PVP nanofibers.

The LUMO and HOMO energy levels of the PEDOT:PSS/PVP nanofiber mat were measured by a CV method. During the measurement, PEDOT:PSS/PVP nanofibers on a Pt plate were used as the working electrode, a Pt plate as the counter electrode, and a Ag/AgCl (0.1 mol/L) standard electrode as the reference electrode. Figure 3(a) shows a typical CV curve of PEDOT:PSS/PVP nanofiber mat (PEDOT:PSS
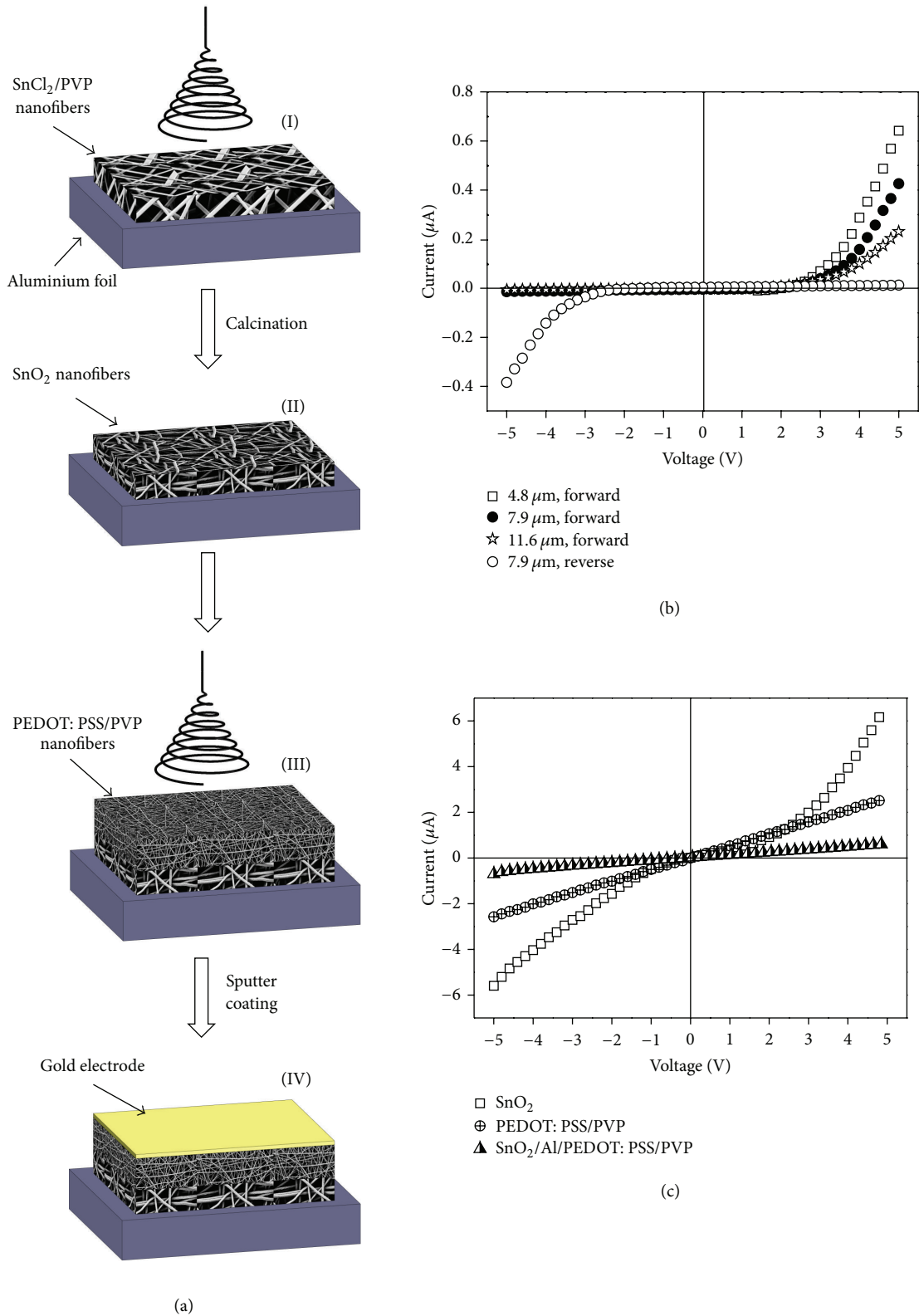
Figure 2: (a) Schematic illustration of device fabrication process, (b) I-V curves of the nanofibrous devices prepared with different thicknesses of the PEDOT:PSS/PVP nanofiber layer (SnO$_2$ nanofiber layer thickness = 4.0 μm), and (c) I-V curves of nanofibers and the electrodes (SnO$_2$ nanofiber layer thickness = 4.0 μm, PEDOT:PSS/PVP nanofiber layer thickness = 7.9 μm).
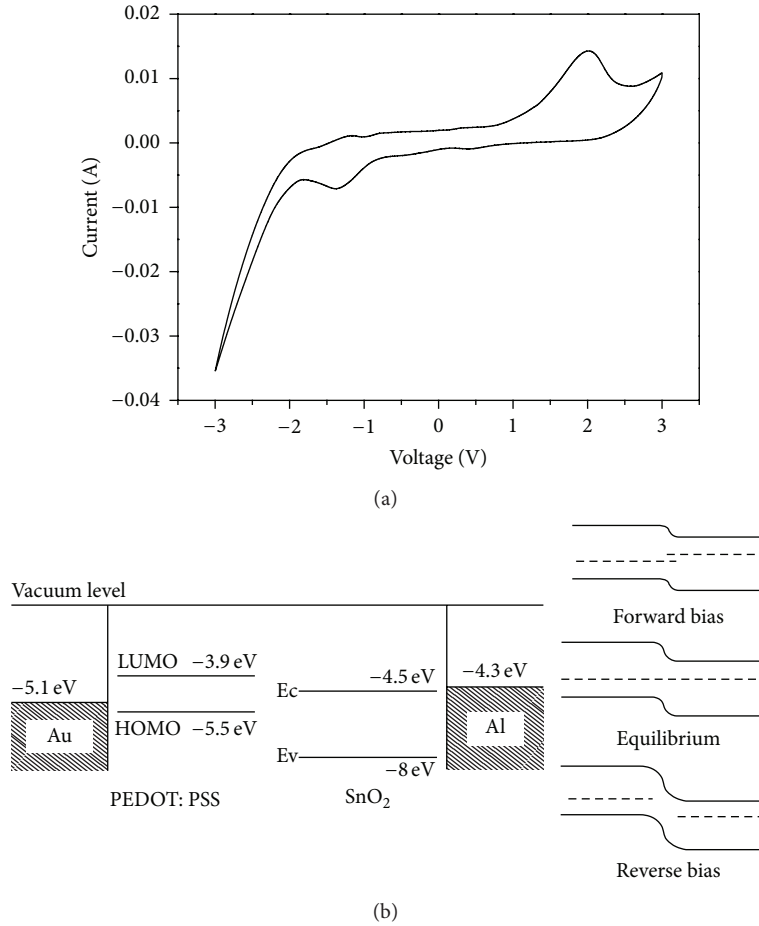
(a)

(b)

FIGURE 3: (a) Cyclic voltammogram curve of the PEDOT:PSS/PVP nanofibers, (b) energy band diagram of the junction.

thickness $= 7.9\,\mu$m). The onset of the first oxidation (E'_{ox}) and reduction (E'_{red}) potential was 0.81 V and -0.75 V, respectively. The LUMO and HOMO levels calculated based on the CV curve were -3.9 eV and -5.5 eV, respectively. Therefore, the bandgap $(E_{\text{g}} = E'_{\text{ox}} + E'_{\text{red}})$ of the PEDOT:PSS/PVP nanofibrous mat is around 1.6 eV, which is similar to that of pure PEDOT:PSS reported [22].

Figure 3(b) shows the energy band diagram of gold, PEDOT:PSS/PVP, SnO$_2$, and aluminium before and after contact. The small difference between the work function of gold (-5.1 eV) and the HOMO level of PEDOT:PSS/PVP made them form an Ohmic contact. Similarly, aluminium and SnO$_2$ also form an Ohmic contact because of the small difference between the SnO$_2$ conduction band and the work function of aluminium (-4.3 eV). Upon close contact between a PEDOT:PSS/PVP and a SnO$_2$ nanofibrous layers, a p-n junction was formed. Electrons flow from the n-type SnO$_2$ nanofibers to p-type PEDOT:PSS/PVP nanofibers. Band bending resulted in a barrier. If the junction is forward connected, positive potential on the PEDOT:PSS/PVP nanofibers lowers their Fermi energy. The decreased barrier allows more charges to cross the junction. On the contrary, a reverse connection results in an increase in the barrier (Figure 3(b)).

To analyse the p-n junction, the standard thermionic emission model was employed, the I-V of which follows the relationship below [22]:

$$I = I_s \left[\exp \frac{qV}{nKT} - 1 \right], \tag{1}$$

where I_s is the saturation current, q is the elementary charge of $1.60217646 \times 10^{-19}$ coulombs, V is the applied voltage, n is the ideality factor, K is the Boltzmann constant of 8.62×10^{-5} eVK^{-1}, and T is the absolute temperature (300 K in this study). The saturation current and the ideality factor can be obtained from the semilog plot of the forward bias current (Figure 4). Reverse saturation current in p-n junction is caused by the migration of minority charge carriers and nearly independent of the reverse bias voltage. By measuring the lowest current value in the curves in Figure 4, the saturation current for the p-n junction with different PEDOT:PSS/PVP layer thicknesses was obtained, being about 7.02×10^{-5}, 5.52×10^{-5}, and $1.39 \times 10^{-5}\,\mu$A for the PEDOT:PSS/PVP thickness of 4.8, 7.9, and 11.6 μm, respectively. The ideality factor can be calculated as the slope of the broken lines in Figure 4, which are the linear fitted to the semilog plots. In this case, three tested p-n junctions had ideality factors of 2.03, 2.13, and 2.29 for the 4.8, 7.9, and
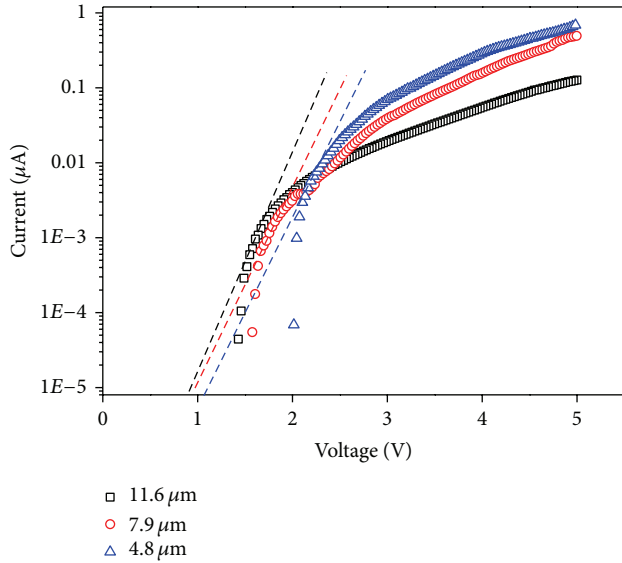
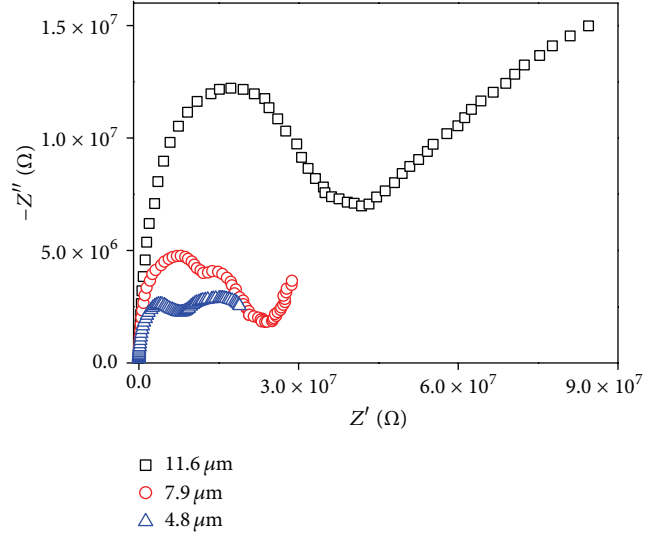FIGURE 4: Semilogarithmic plot of the rectifying current versus applied voltage under forward bias.

FIGURE 5: Electrical impedance spectra of the rectifier devices with different PEDOT:PSS/PVP nanofiber layer thicknesses.

11.6 μm PEDOT:PSS/PVP nanofiber layer, respectively. These ideality factors are slightly higher than the ideal value (1~2) of p-n diodes. This is presumably due to the complex electron transport within the nanofiber matrix.

Once the saturation current is known, the barrier height of the junction (ϕ_b) can be calculated by the following equation [22]:

$$\phi_b = -\frac{KT}{q} \ln \left(\frac{AA^*T^2}{I_s} \right) \qquad (2)$$

Here junction area (A) was set based on the porosity of nanofiber mats and the working area of the device. For most of the electrospun nanofiber mats, the volume porosity was typically over 90% [23]. It is supposed that the chance for nanofibers to contact between two layers is determined by the areal porosity. In the case of nanofiber mat, the areal porosity is supposed to be similar to the volume porosity. The device with 1 cm^2 working area has a junction area $A = 1 \times (1 - 90\%) \times (1 - 90\%) = 0.01$ cm^2. A^* is the effective Richardson constant (120 A/K^2 cm^2). The barrier height of the three junctions was calculated to be 0.90, 0.91, and 0.95 eV for the PEDOT:PSS/PVP nanofiber layer thickness of 4.8, 7.9, and 11.6 μm, respectively.

To further explore the device performance, electrical impedance spectra (EIS) were tested. As shown in Figure 5, there is a complete semicircle at higher frequency range and an incomplete one at lower frequency range, which suggests that both material properties and electrode effect contribute to the device resistance. Bigger semicircle was observed on the spectra when the PEDOT:PSS/PVP layer was thicker, which represented a high electrical resistance of the rectifier. The resistance was obtained from the spectra as 1.89 × 10^7, 2.88 × 10^7, and 8.45 × 10^7 Ω for the PEDOT:PSS/PVP thickness of 4.8, 7.9, and 11.6 μm, respectively. The difference

in rectifying behaviour of three rectifiers should be closely related to the device resistance.

The results of this study have shown that electrospinning is a simple but effective approach to prepare fibrous electronic devices. Electrospun nanofiber webs and novel nanofibrous devices may be useful for development breathable textile electronics. Fibrous rectifiers could also be combined with fibrous power generators for energy harvesting applications. In our previous study, we have reported the mechanical-to-electrical conversion properties of electrospun polyvinyli-dene difluoride (PVDF) nanofiber webs [5]. The nanofibrous rectifier reported in this study could form a flexible candidate to convert AC signals that are generated by the PVDF nanofibers to DC outputs, which will be proven in our further work.

4. Conclusion

A layered fibrous p-n junction has been prepared using a two-step electrospinning technique. The device has an interesting rectifying property with a p-n junction formed between the SnO$_2$ and the PEDOT:PSS/PVP nanofiber layers. The thickness of the PEDOT:PSS/PVP nanofiber layers plays a significant role in determining the rectifying performance of the device. A thicker PEDOT:PSS/PVP nanofiber layer results in higher electrical resistance of the junction. This simple fibrous p-n junction rectifier may find novel applications in electronic textiles, sensors, and energy harvesting devices.

Acknowledgments

References

[1] E. A. Boucher, "Porous materials: structure, properties and capillary phenomena," *Journal of Materials Science*, vol. 11, no. 9, pp. 1734–1750, 1976.

[2] L. Mai, L. Xu, C. Han et al., "Electrospun ultralong hierarchical vanadium oxide nanowires with high performance for lithium ion batteries," *Nano Letters*, vol. 10, no. 11, pp. 4750–4755, 2010.

[3] M. Y. Song, D. K. Kim, K. J. Ihn, S. M. Jo, and D. Y. Kim, "Electrospun TiO_2 electrodes for dye-sensitized solar cells," *Nanotechnology*, vol. 15, no. 12, pp. 1861–1865, 2004.

[4] C. Deng, P. Gong, Q. He et al., "Highly fluorescent TPA-PBPV nanofibers with amplified sensory response to TNT," *Chemical Physics Letters*, vol. 483, no. 4–6, pp. 219–223, 2009.

[5] J. Fang, X. Wang, and T. Lin, "Electrical power generator from randomly oriented electrospun poly(vinylidene fluoride) nanofibre membranes," *Journal of Materials Chemistry*, vol. 21, no. 30, pp. 11088–11091, 2011.

[6] W. Sun, N. P. Kherani, K. D. Hirschman, L. L. Gadeken, and P. M. Fauchet, "A three-dimensional porous silicon *p-n* diode for betavoltaics and photovoltaics," *Advanced Materials*, vol. 17, no. 10, pp. 1230–1233, 2005.

[7] C. Biswas, S. Y. Lee, T. H. Ly, A. Ghosh, Q. N. Dang, and Y. H. Lee, "Chemically doped random network carbon nanotube *p-n* junction diode for rectifier," *ACS Nano*, vol. 5, no. 12, pp. 9817–9823, 2011.

[8] T. Lin, J. Fang, H. Wang, T. Cheng, and X. Wang, "Using chitosan as a thickener for electrospinning dilute PVA solutions to improve fibre uniformity," *Nanotechnology*, vol. 17, no. 15, pp. 3718–3723, 2006.

[9] J. Fang, H. Niu, T. Lin, and X. Wang, "Applications of electrospun nanofibers," *Chinese Science Bulletin*, vol. 53, no. 15, pp. 2265–2286, 2008.

[10] T. Lin, H. Wang, and X. Wang, "Self-crimping bicomponent nanofibers electrospun from polyacrylonitrile and elastomeric polyurethane," *Advanced Materials*, vol. 17, no. 22, pp. 2699–2703, 2005.

[11] J. Fang, H. Wang, H. Niu, T. Lin, and X. Wang, "Evolution of fiber morphology during electrospinning," *Journal of Applied Polymer Science*, vol. 118, no. 5, pp. 2553–2561, 2010.

[12] J. Fang, H. Wang, X. Wang, and T. Lin, "Superhydrophobic nanofibre membranes: effects of particulate coating on hydrophobicity and surface properties," *Journal of the Textile Institute*, vol. 103, no. 9, p. 937, 2012.

[13] T. Lin, H. Wang, H. Wang, and X. Wang, "The charge effect of cationic surfactants on the elimination of fibre beads in the electrospinning of polystyrene," *Nanotechnology*, vol. 15, no. 9, pp. 1375–1381, 2004.

[14] Q. Peng, K. Park, T. Lin, M. Durstock, and L. Dai, "Donor-π-acceptor conjugated copolymers for photovoltaic applications: tuning the open-circuit voltage by adjusting the donor/acceptor ratio," *Journal of Physical Chemistry B*, vol. 112, no. 10, pp. 2801–2808, 2008.

[15] X. Xu, J. Sun, H. Zhang et al., "Effects of Al doping on SnO_2 nanofibers in hydrogen sensor," *Sensors and Actuators B*, vol. 160, no. 1, pp. 858–863, 2011.

[16] O. Martínez, A. G. Bravos, and N. J. Pinto, "Fabrication of poly(vinylidene fluoride-trifluoroethylene)/ poly(3,4-ethylenedioxythiophene) -polystyrene sulfonate composite nanofibers via electro spinning," *Macromolecules*, vol. 42, no. 20, pp. 7924–7929, 2009.

[17] S. M. Sze and K. K. Ng, *Physics of Semiconductor Devices*, Wiley-Interscience, New York, NY, USA, 3rd edition, 2007.

[18] Z. L. Wang, "Functional oxide nanobelts: materials, properties and potential applications in nanosystems and biotechnology," *Annual Review of Physical Chemistry*, vol. 55, pp. 159–196, 2004.

[19] M. Batzill and U. Diebold, "The surface and materials science of tin oxide," *Progress in Surface Science*, vol. 79, no. 2–4, pp. 47–154, 2005.

[20] X. Yong and M. A. A. Schoonen, "The absolute energy positions of conduction and valence bands of selected semiconducting minerals," *American Mineralogist*, vol. 85, no. 3-4, pp. 543–556, 2000.

[21] Y.-Z. Long, M. M. Li, C. Gu et al., "Recent advances in synthesis, physical properties and applications of conducting polymer nanotubes and nanofibers," *Progress in Polymer Science*, vol. 36, no. 10, pp. 1415–1442, 2011.

[22] B. K. Sharma, N. Khare, and S. Ahmad, "A ZnO/PEDOT : PSS based inorganic/organic hetrojunction," *Solid State Communications*, vol. 149, no. 19-20, pp. 771–774, 2009.

[23] X. Liu, T. Lin, J. Fang et al., "*In vivo* wound healing and antibacterial performances of electrospun nanofibre membranes," *Journal of Biomedical Materials Research*, vol. 94, no. 2, pp. 499–508, 2010.

Journal of
Nanotechnology

International Journal of
Corrosion

International Journal of
Polymer Science

Smart Materials
Research

Journal of
Composites

BioMed
Research International

Journal of
Materials

Journal of
Metallurgy

Hindawi

Submit your manuscripts at
http://www.hindawi.com

Journal of
Nanoparticles

Advances in
Materials Science and Engineering

Scientifica

Journal of
Nanomaterials

The Scientific
World Journal

International Journal of
Biomaterials

Journal of
Nanoscience

Journal of
Coatings

Journal of
Crystallography

Journal of
Ceramics

Journal of
Textiles